

# Force distribution in a two dimensional sandpile

Kurt Liffman, Derek Y. C. Chan and Barry D. Hughes

*Department of Mathematics, University of Melbourne, Parkville, Vic. (Australia)*

(Received November 1, 1991; in revised form January 5, 1992)

## Abstract

We have constructed a discrete element computational code which solves the equations of motion that describe particle–particle interactions. As a first example we have applied the code to a two dimensional triangular pile of discrete particles. We take this to be a two dimensional analogue of a conical pile of particulate material. With this simple model, we try to understand—with partial success—the experimental results of Smid and Novosad (*I. Chem. E. Symp.*, 63 (1981) D3/V/1) which show a counter-intuitive dip in the normal stress underneath the highest section of the pile. We also obtain two separate analytic models, one based on recurrence relations and the other on a continuum approximation, to describe the force distribution inside a two dimensional pile of particulate material.

## Introduction

The knowledge of the stress distribution in granular materials is important in our understanding of the mechanical and transport properties of such systems. For instance, granulated materials, such as sugar, fertilizer, and sand are stored in heaps, so if the stress distribution in such configurations is known, then adjustments can be made to minimize the usually deleterious effects of settlement, caking, and comminution. Experimental results that examine the normal and shear stresses at the base of a conical heap of particulate material have been obtained by Smid and Novosad [1]. These experiments demonstrated the counter intuitive result that the normal stress at the base of the pile has a local minimum under the highest point of the conical pile. Curiously, this depression in the normal stress appears to grow with the size of the pile. The smallest piles have a normal stress minimum with a magnitude 20% less than the maximum normal stress, while their largest conical piles gives a stress minimum of magnitude 30% less than the maximum normal stress. Experimental results for the magnitude of the shear stress also showed a minimum under the highest point, which is understandable, since the horizontal forces experienced by a particle resident on the centre line of a conical pile should sum to zero by symmetry.

In this paper we attempt to replicate Smid and Novosad's results by creating a two dimensional analogue of a conical pile of particulate material, which we shall call a sandpile. We study the force structure via simple analytic models and via computer simulation,

where we model the particle–particle interaction in such piles. Other authors [2–5] have embarked upon similar studies, but they have used a method of force analysis which becomes indeterminate when there exists more than two supporting contacts between particles. As part of our analysis, we have used an n-body code that does not place a limitation on the number of particle–particle contacts. The resulting simulation results, and our simple analytic models, allow us to build an intuitive picture of the force distribution in a two dimensional sandpile.

## Experimental

Our simulation studies of particle–particle interactions in a two dimensional pile are based on a standard n-body interaction program [6, 9]. This code solves Newton's equations of motion, in an implicit manner, via the Newton–Raphson method. To speed convergence, the Simultaneous Over Relaxation method is used [6, 7], where the relaxation parameter is given a value between 0.5 and 0.9. In this paper, we assume that all the particles are identical circular disks. Two types of interactions are allowed between the particles. We shall loosely denote these interactions 'hard particle' and 'soft particle' collisions. Hard particle interactions represent the effects of impulsive collisions. Hard particle collision models are, in most cases, an excellent approximation for dynamic particle interactions, but fail to describe the contact force behaviour for particles at rest with each other and the ground. To account

for this behaviour, we allow the particles to interpenetrate once their relative velocities are sufficiently small. It is at this point that the n-body code is used to model the subsequent particle interactions.

#### Hard particle collisions

Although our n-body code does not place a limitation on the number of particle-particle contacts, there are certain circumstances where it is physically viable and computationally convenient to model particle-particle interactions via a two body process. In our code, this occurs when we have dynamic particle-particle or particle-ground interactions, e.g., we may assemble a sandpile by dropping particles onto the ground until a suitably large pile of particles has formed. If the particles are moving 'rapidly' (see eqn. (22)) relative to each other or the ground, it is possible to model their interactions analytically in the following manner.

In the absence of external forces and torques on the colliding particles, linear and angular momentum are conserved. Suppose we have a collision between two particles as shown in Fig. 1. Then conservation of linear momentum gives

$$m_1 \mathbf{c}_1^* + m_2 \mathbf{c}_2^* = m_1 \mathbf{c}_1 + m_2 \mathbf{c}_2 \quad (1)$$

where  $m_i$ ,  $\mathbf{c}_i$ , and  $\mathbf{c}_i^*$  are the mass, velocity before and after collision for particle  $i$ , respectively. Conservation of angular momentum about the contact point  $Q$  implies

$$m_1 \mathbf{r}_1 \times \mathbf{c}_1^* + I_1 \omega_1^* = m_1 \mathbf{r}_1 \times \mathbf{c}_1 + I_1 \omega_1 \quad (2)$$

and

$$m_2 \mathbf{r}_2 \times \mathbf{c}_2^* + I_2 \omega_2^* = m_2 \mathbf{r}_2 \times \mathbf{c}_2 + I_2 \omega_2 \quad (3)$$

where  $\omega_i$ ,  $\omega_i^*$ , and  $I_i$  are the angular velocity before and velocity after the collision, and the moment of inertia about the centre of particle  $i$ , respectively.

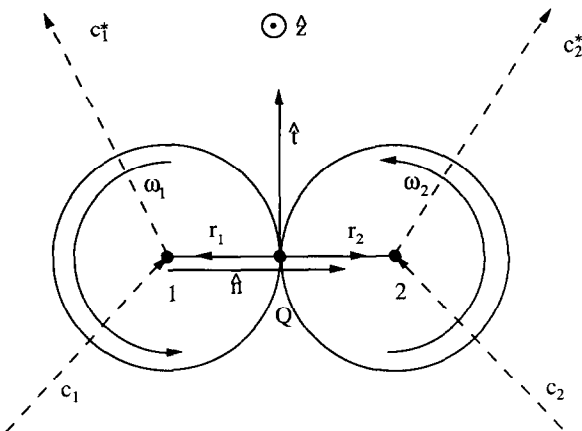


Fig. 1. Particles 1 and 2 collide at point  $Q$  with initial velocities  $\mathbf{c}_1$  and  $\mathbf{c}_2$  and angular velocities  $\omega_1$  and  $\omega_2$  respectively. The unit normal vector, which points along the line joining particles 1 and 2, is denoted by  $\hat{\mathbf{n}}$ . The unit tangent vector,  $\hat{\mathbf{t}}$ , satisfies the equation  $\hat{\mathbf{z}} = \hat{\mathbf{n}} \times \hat{\mathbf{t}}$ , where  $\hat{\mathbf{z}}$  points out of the page.

To describe inelastic collisions, we specify a coefficient of restitution  $\epsilon$ , together with the equation

$$(\mathbf{c}_1^* - \mathbf{c}_2^*) \cdot \hat{\mathbf{n}} = -\epsilon (\mathbf{c}_1 - \mathbf{c}_2) \cdot \hat{\mathbf{n}} \quad (4)$$

which describes the incomplete restitution of translational velocities in the normal ( $\hat{\mathbf{n}}$ ) direction.

The collisional impulse  $P_i$  on the  $i$ th particle is defined by

$$\mathbf{P}_i = m_i (\mathbf{c}_i^* - \mathbf{c}_i) \quad (5)$$

Thus from (1) and (5)

$$\mathbf{P} \equiv \mathbf{P}_1 = m_1 (\mathbf{c}_1^* - \mathbf{c}_1) = m_2 (\mathbf{c}_2 - \mathbf{c}_2^*) = -\mathbf{P}_2 \quad (6)$$

In terms of the collisional impulse  $\mathbf{P}$ , we describe the dynamic sliding friction between the particles

$$P_i^{\text{SLIP}} \equiv \mathbf{P} \cdot \hat{\mathbf{t}} = \mu \mathbf{P} \cdot \hat{\mathbf{n}} \quad (7)$$

where  $\hat{\mathbf{t}}$  is the unit tangent vector that satisfies the equation  $\hat{\mathbf{z}} = \hat{\mathbf{n}} \times \hat{\mathbf{t}}$ , (where  $\hat{\mathbf{z}}$  is a unit vector directed out of the page, see Fig. 1), and  $\mu$  is the coefficient of dynamic friction that needs to be specified. Equation (7) applies if the relative velocity in the tangential plane at the point of contact is reduced, but not entirely eliminated or reversed. We denote this as the SLIP case.

On the other hand, if the relative velocity in the tangential plane at the contact point  $Q$  vanishes as a result of the collision event, then the appropriate friction equation is

$$\mathbf{c}_{12c}^* \cdot \hat{\mathbf{t}} = 0 \quad (8)$$

where  $\mathbf{c}_{12c}$  is the relative velocity between the particles at the point  $Q$ :

$$\mathbf{c}_{12c} = \mathbf{c}_1 + \mathbf{r}_1 \times \omega_1 - \mathbf{c}_2 - \mathbf{r}_2 \times \omega_2 \quad (9)$$

A situation where eqn. (8) is applicable is called a NOSLIP case.

Thus the effects of inelastic collisions on changes in the translational velocities in the normal direction are modelled by eqn. (4), while eqns. (7) and (8) describe two possible models for changes in the tangential components of particle velocities.

From eqn. (1)

$$\mathbf{c}_2^* = \mathbf{c}_2 + m (\mathbf{c}_1 - \mathbf{c}_1^*) \quad (10)$$

where  $m = m_1/m_2$ . Substitution of (1) into (4) provides an expression for  $\mathbf{c}_1^* \cdot \hat{\mathbf{n}}$ :

$$\mathbf{c}_1^* \cdot \hat{\mathbf{n}} = [(m - \epsilon) \mathbf{c}_1 \cdot \hat{\mathbf{n}} + (1 + \epsilon) \mathbf{c}_2 \cdot \hat{\mathbf{n}}] / (1 + m) \quad (11)$$

If we combine (11) with the definition of  $P$  (eqn. (6)) we obtain

$$P_n \equiv \mathbf{P} \cdot \hat{\mathbf{n}} = \frac{m_1 m_2}{(m_1 + m_2)} (1 + \epsilon) (\mathbf{c}_2 - \mathbf{c}_1) \cdot \hat{\mathbf{n}} \quad (12)$$

which is true for both the SLIP and NOSLIP cases.

The angular velocities  $\omega_1$  and  $\omega_2$  can be readily determined from eqns. (2) and (3):

$$\omega_1^* = \omega_1 + m_1 \mathbf{r}_1 \times (\mathbf{c}_1 - \mathbf{c}_1^*) / I_1 = \omega_1 - \mathbf{r}_1 \times \mathbf{P} / I_1 \quad (13)$$

and

$$\omega_2^* = \omega_2 + m_2 \mathbf{r}_2 \times (\mathbf{c}_2 - \mathbf{c}_2^*) / I_2 = \omega_2 - \mathbf{r}_2 \times \mathbf{P} / I_2 \quad (14)$$

For the NOSLIP case, substitution of eqns. (9), (13), (14) into eqn. (8) gives

$$\begin{aligned} & \mathbf{c}_1^* \cdot \hat{\mathbf{t}} \\ &= \frac{\left( \mathbf{c}_2 \cdot \hat{\mathbf{t}} + \left( m + \frac{m_1 r_2^2}{I_2} + \frac{m_1 r_1^2}{I_1} \right) \mathbf{c}_1 \cdot \hat{\mathbf{t}} + (\mathbf{r}_2 \times \omega_2) \cdot \hat{\mathbf{t}} - (\mathbf{r}_1 \times \omega_1) \cdot \hat{\mathbf{t}} \right)}{\left( 1 + m + \frac{m_1 r_2^2}{I_2} + \frac{m_1 r_1^2}{I_1} \right)} \end{aligned} \quad (15)$$

It follows from (15) and (6) that

$$P_t^{\text{NOSLIP}} = \frac{m_1 (\mathbf{c}_2 - \mathbf{c}_1 + \mathbf{r}_2 \times \omega_2 - \mathbf{r}_1 \times \omega_1) \cdot \hat{\mathbf{t}}}{\left( 1 + m + \frac{m_1 r_2^2}{I_2} + \frac{m_1 r_1^2}{I_1} \right)} \quad (16)$$

where we have from Fig. 1

$$(\mathbf{r}_2 \times \omega_2) \cdot \hat{\mathbf{t}} = -r_2 \omega_2 \quad (17)$$

and

$$(\mathbf{r}_1 \times \omega_1) \cdot \hat{\mathbf{t}} = r_1 \omega_1 \quad (18)$$

To determine whether the SLIP or NOSLIP case is appropriate, we use the physical constraint that the tangential impulse must always be less than  $P_t^{\text{NOSLIP}}$ . Thus,

$$\begin{aligned} P_t^{\text{NOSLIP}} > P_t^{\text{SLIP}} &\Rightarrow P_t = P_t^{\text{SLIP}} \\ P_t^{\text{NOSLIP}} \leq P_t^{\text{SLIP}} &\Rightarrow P_t = P_t^{\text{NOSLIP}} \end{aligned} \quad (19)$$

Once we have determined  $P (= P_n \hat{\mathbf{n}} + P_t \hat{\mathbf{t}})$ , we can evaluate  $\mathbf{c}_1^*$ ,  $\mathbf{c}_2^*$  from eqn. (6) and  $\omega_1^*$ ,  $\omega_2^*$  from eqns. (13) and (14) respectively.

To transform to other coordinate systems, e.g. cartesian, we note that in a two dimensional cartesian system  $\hat{\mathbf{n}} = (n_x, n_y)$  and  $\hat{\mathbf{t}} = (-n_y, n_x)$ . Thus

$$P_x = P_n n_x - P_t n_y \quad (20)$$

and

$$P_y = P_n n_y + P_t n_x \quad (21)$$

Solutions for the velocities follow as before.

Although we shall only consider identical particles in this paper, the results given here are valid for non-identical particles. A more complete description of hard body collisions, particularly for particles of arbitrary shape, may be found in Hopkins [8].

### Soft body collisions

A soft body collision means that the particles can interpenetrate. This is a necessary attribute when we wish to study the force distribution in a static collection of particles, because computing the forces in a static structure is not possible if we use the hard body collision physics outlined above. A repulsive force, which is dependent on the interpenetration distance, can be easily programmed into a general n-body code.

In our simulation study, the particle collision automatically changes from hard to soft if the time step  $\Delta t$  satisfies the condition

$$\Delta t > m |\mathbf{v} \cdot \hat{\mathbf{n}}| / |\mathbf{F} \cdot \hat{\mathbf{n}}| \quad \text{if } \mathbf{v} \cdot \hat{\mathbf{n}} \geq 0, \text{ and } \mathbf{F} \cdot \hat{\mathbf{n}} < 0 \quad (22)$$

where  $m$  is the mass of the particle,  $\hat{\mathbf{n}}$  is a normal to an arbitrary surface, and  $\mathbf{F}$  is the resultant force on the particle which has a component antiparallel to  $\hat{\mathbf{n}}$  (see Fig. 2). An intuitive understanding of eqn. (22) is obtained if we consider  $\mathbf{F}$  to be the force of gravity on a particle in contact with the ground. If we assume that the particle has a zero initial velocity, i.e.  $\mathbf{v} = \mathbf{0}$ , then the velocity of the particle (in the absence of a resistive normal force from the ground) after a time  $\Delta t$  will be  $-g\Delta t$  (taking the 'up' direction as positive). This undesirable situation, of a solid particle moving through solid ground, would occur for all  $\Delta t > 0$ . Similarly if there existed a component of  $\mathbf{v}$  in the 'up' direction then the particle would again move through the ground if the timestep  $\Delta t > |\mathbf{v} \cdot \hat{\mathbf{n}}| / g$ . The necessity for a resistive normal force in such a circumstance is obvious, and the code automatically changes from a hard to a soft body interaction to allow this normal force to be created.

To simulate soft body interactions, we adopt the coordinate system shown in Fig. 3. Figure 3 differs from Fig. 1 in that the direction of vectors  $\hat{\mathbf{n}}$  and  $\hat{\mathbf{t}}$  have been reversed. This slight change is convenient, because to model the soft body collision, we must solve Newton's equation of motion and so we require the resultant force acting on particle 1 from particle 2, which will act in the direction of  $\hat{\mathbf{n}}$ .

We chose the potential energy of the particle-particle interaction to be

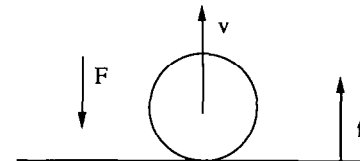


Fig. 2. To determine when the hard particle turns into a soft particle, we can use the simple example given in this figure. If the initial velocity of the particle away from the surface is smaller than the velocity of the particle, acquired in a timestep  $\Delta t$ , due to the component of force acting towards the surface, then the particle will penetrate the surface and become soft.

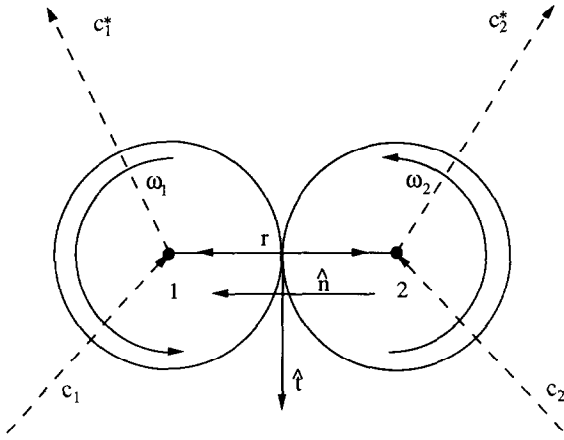


Fig. 3. The coordinate system used for soft particle collisions.

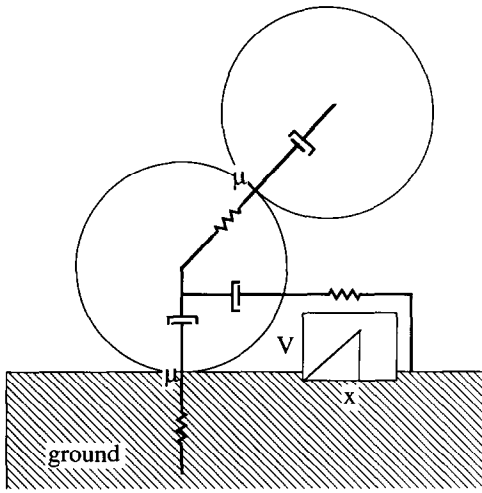


Fig. 4. Schematic depiction of the forces that are simulated by our computer code for particle-particle and particle-ground contacts. Particle-particle interactions can be represented as a damped (repulsive) spring acting along the line joining the centres of the two particles. The repulsive spring force arises when the two particles interpenetrate. Additional tangential forces from rolling and slipping friction are denoted by the symbol  $\mu$ . Particle-ground forces are simulated in exactly the same manner, with an additional static friction term. We simulate static friction via a damped (attractive) spring, which 'breaks' once the particle has moved a small distance away from its initial position. This is shown in the magnitude of the potential energy ( $V$ ) vs. distance ( $x$ ) graph.

$$V = \begin{cases} 0 & \text{for } r \geq \sigma \\ K_s(\sigma - r)^2/2 & \text{for } r < \sigma \end{cases} \quad (23)$$

where  $\sigma$  is the diameter of the particle,  $r$  is the distance between the centres of the particles and  $K_s$  is a spring constant. Thus, when the particles interpenetrate, a spring effectively arises between them and forces them apart (see Fig. 4). From eqn. (23), we can obtain a difference formula for the repulsive force

$$f_k = - \frac{V(r_{k+1}) - V(r_k)}{r_{k+1} - r_k} = K_s[\sigma - (r_{k+1} + r_k)/2] \quad (24)$$

where  $f_k$  and  $r_k$  are the force and distance between the centres of the particles at the  $k^{\text{th}}$  timestep, respectively. This difference equation, coupled with the Newton-Raphson method, allows us to compute the repulsive normal force. Our difference equations are so constructed that energy is automatically conserved within the system [9]. To simulate real physical collisions, we require additional dissipative frictional forces. With this in mind, our repulsive force of eqn. (24), which acts in the normal  $\hat{n}$  direction, is given an extra damping term:

$$F_k^{\text{norm}} = K_s[\sigma - (r_{k+1} + r_k)/2] - K_D V_{\text{norm}} \quad (25)$$

where  $K_D$  is a damping constant, and  $V_{\text{norm}}$  is the component of the relative velocity  $\mathbf{v}_1 - \mathbf{v}_2$  in the  $\hat{n}$  direction:

$$V_{\text{norm}} = (v_{1x} - v_{2x})n_x + (v_{1y} - v_{2y})n_y \quad (26)$$

Clearly, with this form of damping, it is possible to damp out all motion parallel to  $\hat{n}$ .

To damp out motion parallel to  $\hat{t}$ , one must introduce sliding, rolling and static friction. Our sliding friction takes the form

$$F_{\text{slip}} = -K_{\text{slip}} v_{\text{tang}} \quad (27)$$

where  $K_{\text{slip}}$  is the coefficient of sliding friction, and  $v_{\text{tang}}$  is the component of the relative velocity  $\mathbf{v}_1 - \mathbf{v}_2$  in the  $\hat{t}$  direction:

$$\begin{aligned} v_{\text{tang}} &= (\mathbf{v}_1 - \mathbf{v}_2 + \mathbf{r}_1 \times \boldsymbol{\omega}_1 - \mathbf{r}_2 \times \boldsymbol{\omega}_2) \cdot \hat{t} \\ &= -(v_{1x} - v_{2x})n_y + (v_{1y} - v_{2y})n_x - r_1\omega_1 - r_2\omega_2 \end{aligned} \quad (28)$$

Our form for rolling friction is based on that given by Witters and Duymelinck [10]

$$F_{\text{roll}} = -\mu_{\text{roll}} F_k^{\text{norm}} \hat{t} \quad (29)$$

where  $\mu_{\text{roll}}$  is the coefficient of rolling friction, and  $F_k^{\text{norm}}$  is shown in eqn. (25). To determine whether the particle is rolling, sliding or both, we simply take the minimum magnitude of eqns. (27) and (29).

For the purposes of our study, it is only necessary to consider static friction when the particle is in contact with the ground and the particle begins to move from rest. We simulate static friction by creating a potential well underneath the particle which opposes any motion parallel to the ground. The equation describing the static friction force:

$$F_k^{\text{static}} = \begin{cases} 0 & \text{for } |x - x_0| > a \\ -\frac{\mu_{\text{static}} N}{a} \left( \frac{(x_{k+1} - x_k)}{2} - x_0 \right) & \text{for } |x - x_0| \leq a \end{cases} \quad (30)$$

where  $x_0$  is the  $x$  position of the particle at rest on the ground,  $a$  is the half-width of the potential well,  $\mu_{\text{static}}$  is the coefficient of static friction, and  $N$  is the normal force of the ground on the particle.  $N$  is computed via eqn. (25).

By combining all the forces in eqns. (25), (27), (29), and (30) we can compute the total force that acts through the centre:

$$\mathbf{F}_{\text{total}} = F_n \hat{\mathbf{n}} + F_t \hat{\mathbf{t}} \quad (31)$$

where  $F_n$  is given by eqn. (25) and  $F_t$  for a particle in contact with particles above the ground is given by

$$F_t = \min(F_{\text{slip}}, F_{\text{roll}}) \quad (32)$$

while  $F_t$  for a particle in soft contact with the ground is

$$F_t = \min(F_{\text{slip}}, F_{\text{roll}}) + F_k^{\text{static}} \quad (33)$$

To convert from the  $\hat{\mathbf{n}}$  and  $\hat{\mathbf{t}}$  directions to the usual cartesian coordinates we use the equations

$$F_x = F_n n_x - F_t n_y \quad (34)$$

$$F_y = F_n n_y + F_t n_x \quad (35)$$

and to compute the moment of force ( $\tau$ ) that makes the particle roll, we have:

$$\tau = \sigma F_{\text{slip}} / 2 \quad (36)$$

from which we can compute the angular velocities of the particles.

All the above information is presented schematically in Fig. 4, which allows one to obtain an intuitive understanding of the mechanisms used in our computer code for simulating soft body interactions. A more complete description of soft body interactions may be found in Cundall and Strack [11].

## Results

### A close packed equilateral sandpile-analytic model

We can obtain simple analytic results for the force distribution in a two dimensional system, if we consider a sandpile where all the particles are 'hard', *i.e.* they suffer no change in size as they are subjected to an external force, and the particles lie on a grid as shown in Fig. 5. Unlike the normal cartesian system, the  $x$ ,  $y$  axes shown in Fig. 5 are not mutually orthogonal. We are motivated to assume this grid system by noting that the basic force unit is a system of three particles (see Fig. 5). The static forces will propagate through the contact points and thus at angle to the gravitational force  $g$ . If we analyze the forces acting on a particle at  $(x, y)$ , we find by resolving forces in the horizontal direction,

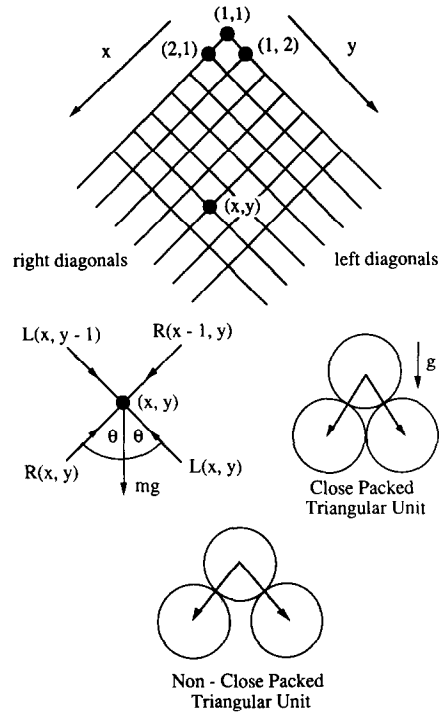


Fig. 5. To study the distribution of forces in a sandpile, we have created a coordinate grid where every intersection point can contain a particle. The forces propagate through the particle contact points which lie along the coordinate lines. Unlike normal cartesian coordinates, our grid lines are not mutually orthogonal. We are motivated to assume this grid system by noting that the basic force unit is a system of three particles. The static forces will propagate through the contact points and thus at angle to the gravitational force  $g$ . If we analyze the forces through an arbitrary particle located at  $(x, y)$ , we obtain eqns. (37) to (41). For close packed disks, with equal radii, the angle  $\theta$  will have the value  $\pi/6$ . If the disks are not closely packed, then the angle  $\theta$  may be greater than  $\pi/6$ .

$$L(x, y-1) + R(x, y) - L(x, y) - R(x-1, y) = 0 \quad (37)$$

where  $L$  stands for forces directed along the left diagonal and, similarly,  $R$  stands for forces directed along the right diagonal. The vertical component of the force satisfies the equation

$$L(x, y) + R(x, y) - L(x, y-1) - R(x-1, y) = W \quad (38)$$

where  $W = mg / \cos \theta$ . By adding and subtracting eqn. (37) from eqn. (38), and setting

$$L(x, 0) = R(0, y) = 0 \quad (39)$$

we can obtain recurrence relations for  $L$  and  $R$ , which have the solutions

$$L(x, y) = Wy/2 \quad (40)$$

and

$$R(x, y) = Wx/2 \quad (41)$$

A particle on the ground will experience a normal force plus a frictional force. From an analysis based on Fig. 6, we find that the normal force ( $N$ ) exerted by the ground on the particle is

$$N = (k + 1)mg/2 \tag{42}$$

where  $k$  is the number of layers in the pile. Thus the normal force is constant for all particles in contact with the ground for this theoretical pile. The horizontal force that the particle exerts on the ground ( $H$ ) is given by the formula

$$H = mg \tan \theta [2i - k - 1]/2 \tag{43}$$

For  $\theta = \pi/6$ , i.e. for close packed identical disks, eqn. (43) becomes

$$H = \frac{mg[2i - k - 1]}{2\sqrt{3}} \tag{44}$$

$H$  has a maximum absolute magnitude when  $i = 1$  and  $k$ . Also,  $H = 0$  when  $i = (k + 1)/2$  ( $k$  odd).

*A close packed equilateral sandpile—computational model*

As a first test of our computational model, we create an equilateral pile consisting of 1035 identical soft particles (Fig. 7). Each particle in the pile satisfies the dimensionless equation

$$mg/K_s \Delta x = 1 \tag{45}$$

where  $K_s$  is the spring constant, and  $\Delta x$  is the distance a soft particle will sink into the ground due to the force of its own weight. Equation (45) is simply a force balance equation, where the spring force balances the weight force of the particle. In our simulations, it is computationally convenient to choose

$$mg/K_s \sigma = 10^{-4}, \text{ or } \Delta x = 10^{-4} \sigma \tag{46}$$

where  $\sigma$  is the diameter of the particle. In other words our 'soft' particle will, under its own weight, sink into the ground a distance of  $10^{-4} \sigma$ . Our 'soft' particle is thus a good approximation to a 'hard' particle only

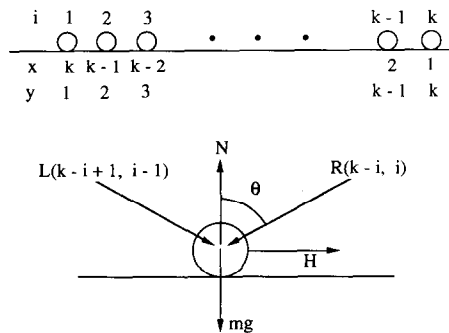


Fig. 6. The coordinate numbers and force structure for particles in contact with the ground.

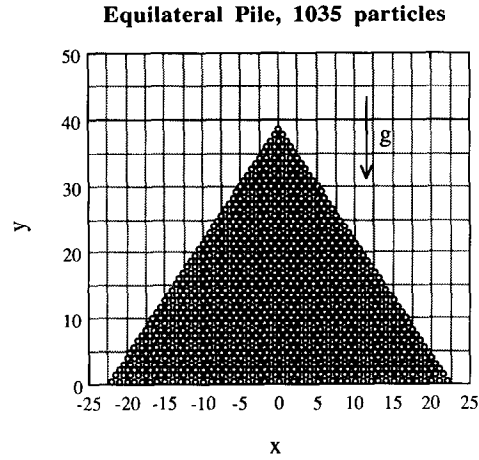


Fig. 7. As the first trial for the force code, the force structure in this equilateral close packed pile of 1035 particles is analyzed. There are 45 layers of particles in this pile, and the same number in contact with the ground. The unit of length is the diameter of a particle ( $\sigma$ ).

down to one part in  $10^4$ , since a hard particle would not sink into the ground at all. Indeed, the ground particles in the equilateral pile of Fig. 7 will have to support the weight of their higher fellow particles, which (from eqn. (42)) means that they will sink a distance of about  $2.3 \times 10^{-3} \sigma$  into the ground. Thus the expected relative difference in force structure between our pile of 'soft' particles and the theoretical pile of 'hard' particles should be of order  $2.3 \times 10^{-3}$ .

In Figs. 8 and 9, we plot the normal and horizontal forces obtained from the code and from eqns. (42) and (44). As can be seen, the relative difference between the predictions of eqns. (42) and (44) with the computational model is less than 1%. The difference is obvious in Fig. 8, but is not seen in Fig. 9 due to the larger size scale over which the horizontal force results are displayed.

In our analytic model, we have assumed that the forces act in diagonal lines thereby ignoring any possible contacts between particles on the same level. We can use our computer model to determine the veracity of this assumption for the spring constants chosen in this example. Suppose we study the force structure of a particle situated at an arbitrary point  $(x, y)$  in the pile (see Fig. 5). The force coming from above and from the left would be  $L(x, y - 1)$ . Similarly the force from above and the right would be  $R(x - 1, y)$ . Using eqns. (40) and (41) we can write

$$L(x, y - 1) > R(x - 1, y) \text{ implies } y > x \tag{47}$$

and

$$L(x, y - 1) \leq R(x - 1, y) \text{ implies } y \leq x \tag{48}$$

So we should expect that the left and right hand forces should be equal down the central axis of the pile. On

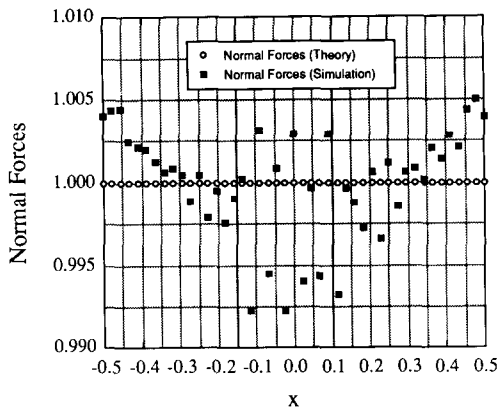


Fig. 8. The analytic prediction of eqn. (42) vs. the results from the computational model for normal forces in an equilateral pile, where the forces have been normalized to the theoretically expected value. Also, the base length of the pile has been normalized to 1. The difference between the two results is (as expected) at the 1% level and is due to the compressibility of the computer particles.

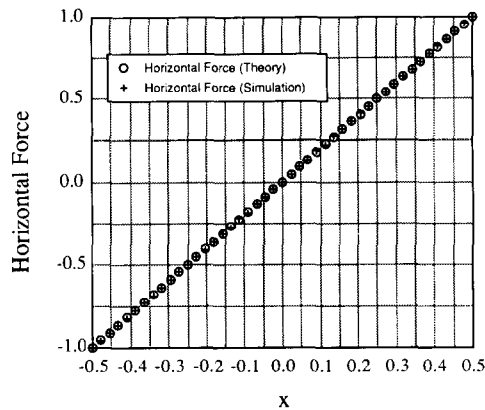


Fig. 9. The analytic prediction of eqn. (44) vs. the results from the computational model for the horizontal forces the equilateral pile exerts on the ground. The forces have been normalized to the maximum magnitude of the theoretically predicted values, and the base length of the pile has been normalized to 1.

the left hand side of the pile, the forces on the right diagonal (*i.e.* in the  $x$  direction) will be stronger than the forces on the left diagonal ( $y$  direction) and vice versa. One of the advantages of our computational model is our ability to visualize all the forces acting on each of the particles. This allows us to view both the strongest and the weakest of the forces acting on each particle. In Figs. 10(a) and 10(b), we display the lines of maximum and minimum force, respectively, between each particle pair. As our analysis with eqns. (47) and (48) predicts, each separate line element between any two particles join up to form long lines that are parallel or make an angle of  $\pi/3$  to the slope of our equilateral close packed sandpile. This is not surprising since, as mentioned previously, our funda-

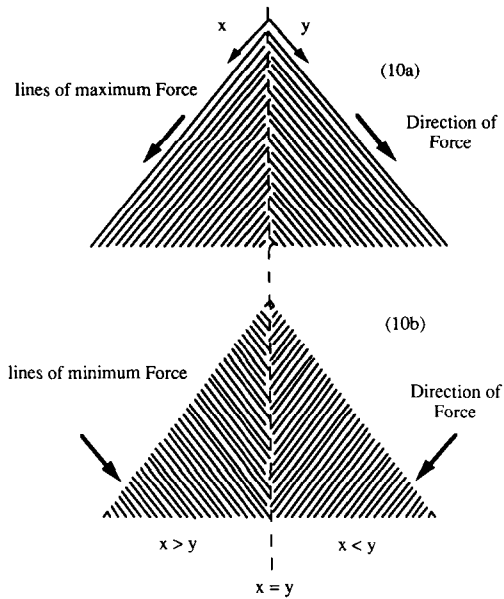


Fig. 10(a) and (b). Lines of force in the equilateral pile shown in Fig. 7 as determined from our n-body code. The behaviour of the lines of force from the simulation are consistent with the predictions from our simple analytic model. The direction and magnitude of the lines of force are dependent on position in the pile as outlined in eqns. (47) and (48). For example if  $x > y$ , then the strongest forces are parallel to the  $x$  axis (Fig. 10(a)), while the weakest forces are parallel to the  $y$  axis (Fig. 10(b)). Force balance occurs along the centre line at  $x = y$ , and the pattern is reversed when  $x < y$ .

mental force unit is an equilateral triangle of particles (Fig. 5). As is consistent with our theoretical model, no horizontal forces are found between neighbouring particles in this sandpile.

*A close packed sandpile with arbitrary slope – theory*

From the comparisons between the analytic and computational results for a close packed equilateral sandpile, it appears that we have achieved a relatively good understanding of a perfect equilateral pile. However, for a general pile of base width  $B$  and a general angle of repose  $\alpha < \pi/3$ , then our analytic model breaks down, since there is no longer a particle at every lattice point of our grid. It is still possible to work out the propagation of force down each diagonal, but we no longer obtain simple recurrence relations like eqns. (37) and (38). The problem becomes amenable to an approximate solution, however, if we take the continuum limit and make each of our particles, nearly, infinitesimal in size. Thus we assume that the force still propagates in a diagonal fashion (see Fig. 11), where the angle between the line of force and the ground is  $\pi/3$  or  $2\pi/3$ . This is true if our nearly infinitesimal particles have equal radii, are incompressible, and are close packed.

We can now characterize a linear mass density  $\chi$  along each diagonal line. For example  $\chi$  can have the form:  $\chi = m/\sigma$ . Thus the mass of a line of length  $l$  is

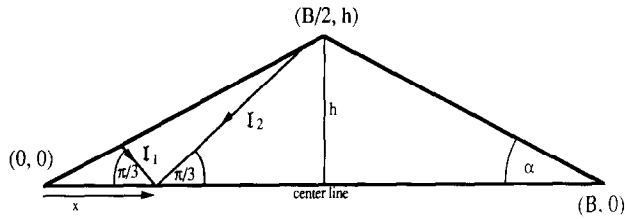


Fig. 11. An isosceles triangle outlines our 'continuum particulate' pile. The triangle has a base of length  $B$ , a height  $h$  and an angle of repose  $\alpha$  which is strictly less than  $\pi/3$ . The force is assumed to propagate along diagonal lines of length  $I_1$  and  $I_2$ , where each line makes an angle of  $2\pi/3$ , and  $\pi/3$  with the horizontal. The intersection point of lines  $I_1$  and  $I_2$  is a distance  $x$  from the origin.

$\chi l$  and the total force directed down the diagonal is, by analogy with eqns. (40) and (41) for  $\theta = \pi/3$ ,  $\chi l g / \sqrt{3}$ . It is not difficult to show that for  $x \leq x_c \equiv h[\cot \alpha - 1/\sqrt{3}]$

$$I_1 = x \sin \alpha / \sin(2\pi/3 - \alpha) \tag{49}$$

and

$$I_2 = x \sin \alpha / \sin(\pi/3 - \alpha) \tag{50}$$

If  $x_c < x < B/2$ , then  $I_1$  remains unchanged, but the  $I_2$  line intercepts the other slope of the sandpile and its length becomes

$$I_2 = (B - x) \sin \alpha / \sin(2\pi/3 - \alpha) \tag{51}$$

At  $x$ , the point of intersection of the diagonal lines, the normal force ( $N$ ) of the ground on the pile satisfies

$$N = \chi g (I_1 + I_2) / 2 \tag{52}$$

and the horizontal force ( $H$ ) of the pile on the ground is

$$H = \chi g (I_1 - I_2) / (2\sqrt{3}) \tag{53}$$

Substitution of (49), (50), and (51) into (52), and (53) plus the symmetric nature of the pile gives:

For  $0 \leq x \leq x_c$

$$N = \frac{\sqrt{3} x \chi g \sin \alpha \cos \alpha}{2 \sin(2\pi/3 - \alpha) \sin(\pi/3 - \alpha)} \tag{54}$$

and

$$H = \frac{-x \chi g \sin^2 \alpha}{2\sqrt{3} \sin(2\pi/3 - \alpha) \sin(\pi/3 - \alpha)} \tag{55}$$

For  $x_c < x < B - x_c$

$$N = \frac{\chi g B \sin \alpha}{2 \sin(2\pi/3 - \alpha)} \tag{56}$$

and

$$H = \frac{\chi g (x - B/2) \sin \alpha}{\sqrt{3} \sin(2\pi/3 - \alpha)} \tag{57}$$

Finally, for  $B - x_c < x < B$

$$N = \frac{\sqrt{3}(B-x)\chi g \sin \alpha \cos \alpha}{2 \sin(2\pi/3 - \alpha) \sin(\pi/3 - \alpha)} \tag{58}$$

and

$$H = \frac{(B-x)\chi g \sin^2 \alpha}{2\sqrt{3} \sin(2\pi/3 - \alpha) \sin(\pi/3 - \alpha)} \tag{59}$$

*A close packed sandpile with arbitrary slope – computational model*

We compare theory to our computational results by simulating piles of material with different angles of repose ( $\alpha$ ). In particular, we consider the values  $\alpha = 55^\circ$ ,  $50^\circ$ ,  $45^\circ$ , and  $30^\circ$ . Also, noting that

$$\chi = m/\sigma \tag{60}$$

we can express  $\chi$  in terms of eqns. (45) and (46). Finally, for convenience, we normalize  $B$  to take the value 1.

To provide an example of what these non-equilateral sandpiles look like, we show the  $55^\circ$  pile in Fig. 12. In Figs. 13 and 14 we compare the analytic versus computed results for the normal and horizontal forces, respectively, along the base of the different piles. In Fig. 13, the circles represent the normal forces obtained from the computer code, while the lines give the analytically derived forces from eqns. (54), (56), and (58). All the forces are normalized to the maximum force value obtained from the computer code. The difference between the theoretically expected normal forces and those obtained from the computer simulation is partially due to the finite size of the particles in the computer pile. The normal forces obtained from the simulation include the full weight of the particles on the base of the pile, while the analytic continuum model ignores

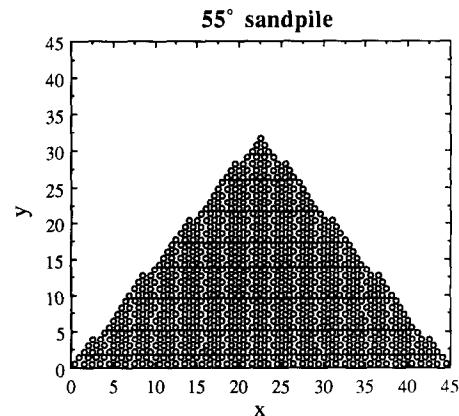


Fig. 12. This pile has an angle of repose of  $55^\circ$ . Because the pile is made of discrete particle, the sides are composed of a number of sloping steps. The unit of length in this picture is the diameter of the particles.

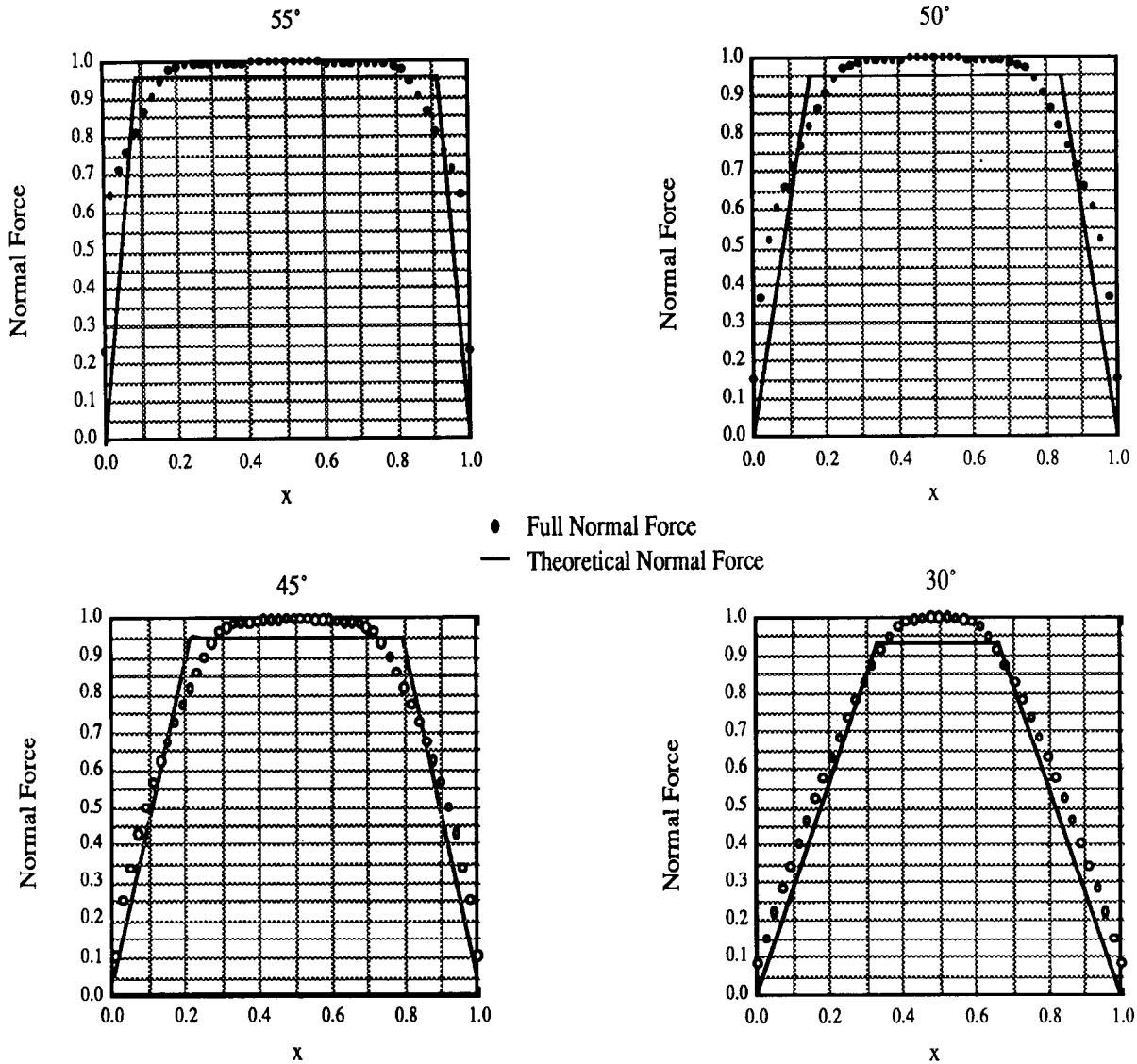


Fig. 13. The computed and analytic normal forces for piles of particles with  $\alpha=30^\circ$ ,  $45^\circ$ ,  $50^\circ$ , and  $55^\circ$ . The circles represent the normal forces obtained from the computer code, and the lines show the forces from eqns. (54), (56), and (58). All the forces are normalized to the maximum force value obtained from the computer code. The difference between the theoretically expected normal forces and those obtained from the computer simulation is partially due to the finite nature of the computer pile. The normal forces obtained from the simulation include the full weight of the particles on the base of the pile, while the analytic continuum model ignores this contribution. Also the size of the particle is approximately a fiftieth of the pile size, while the analytic results assume that the particles are infinitesimal compared to the size of the pile.

this contribution. Also the size of the particle is approximately a fiftieth of the pile size, while the analytic results assume that the particles are infinitesimal compared to the size of the pile. If we increase the number of particles in the pile, the difference between the models decreases (see Fig. 15).

In Fig. 14, the circular points represent the horizontal forces the pile exerts on the ground as obtained from the computer code, while the lines show the analytically derived forces from eqns. (55), (57) and (59). Again, all the forces are normalized to the maximum force value obtained from the computer code. Interestingly,

the central portion of the force profile for both the computer simulation and the analytic theory (eqn. (57)) is dependent on the angle of repose of the pile. The differences between the analytic and computational force profiles are not due to the fact that we are comparing a continuum analytic model to a discrete particle model, since when we increase the number of particles, we still obtain basically the same horizontal pile-ground force profiles from our computer results (see Fig. 15). The fundamental reason for the difference is, we believe, due to our assumption that all the forces propagate at an angle of  $\pi/3$  or  $2\pi/3$  to the horizontal

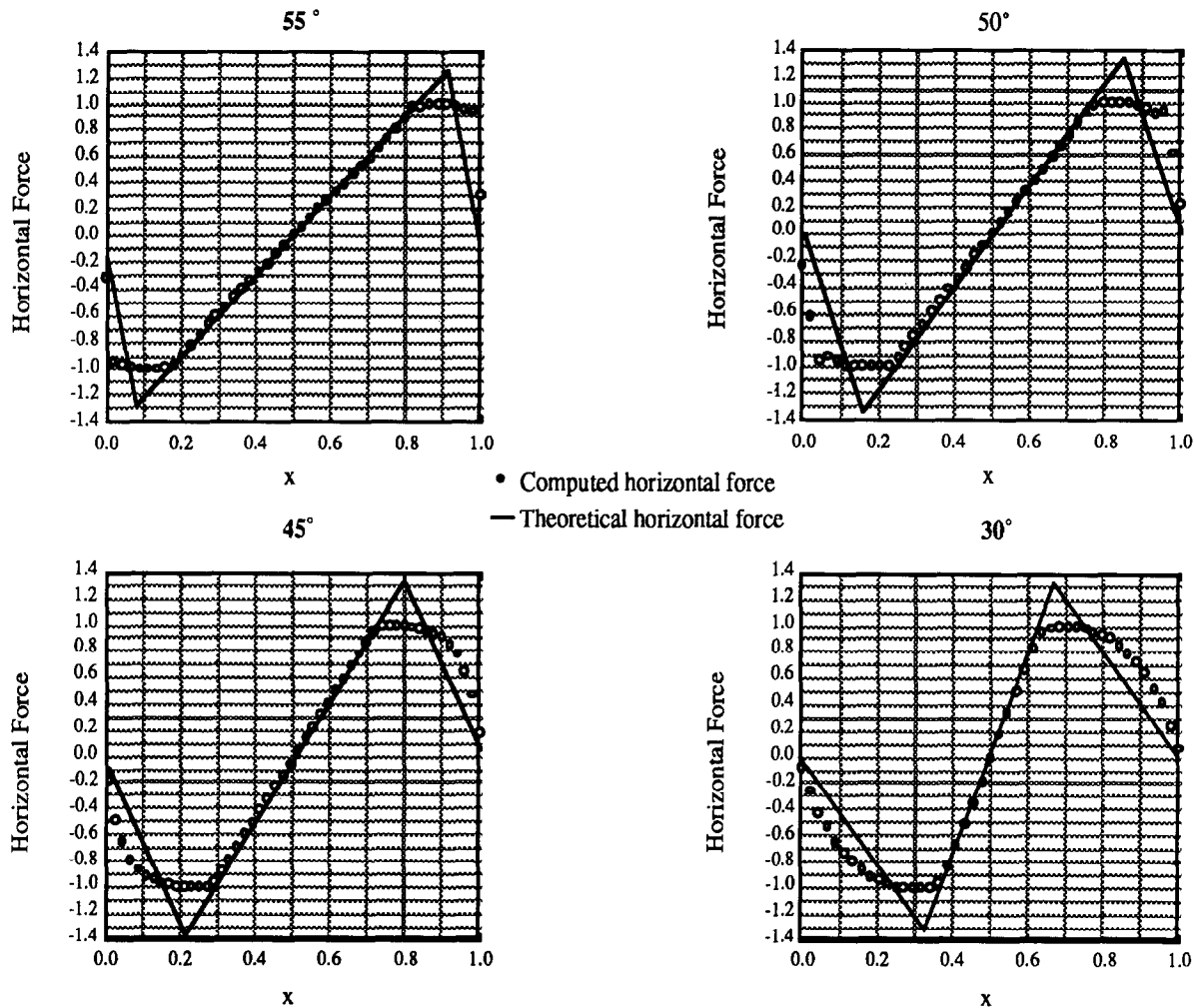


Fig. 14. The computed and theoretical horizontal forces that piles of particles with  $\alpha = 30^\circ$ ,  $45^\circ$ ,  $50^\circ$ , and  $55^\circ$  exert on the ground. The circular dots represent the horizontal forces obtained from the computer code. The dark lines represent the analytically derived forces from eqns. (55), (57), and (59). Note that the central portion of the force profile for both the computer simulation and the analytic theory is dependent on the angle of repose of the pile.

in the analytic model, while the results of our computational model suggests that some of the forces propagate horizontally between neighbouring particles. This can be seen in Fig. 16, where we show the force lines of weakest and strongest forces in the  $\alpha = 30^\circ$  pile, with similar results being true for the  $55^\circ$ ,  $50^\circ$ , and  $45^\circ$  piles.

#### Experiment versus computer model

As mentioned previously, the only experiment that has been done to measure the stress distribution in sandpiles is that of Smid and Novosad [1]. We have taken their results for the largest pile of sand in their experiment, normalized them and then compared them to the normalized results from our computational model. The angle of repose for Smid and Novosad's sand pile was  $32.6^\circ$  which we have duplicated in our computer model. The comparison is shown in Fig. 17, where it

can be seen that the central 'linear' portion of the horizontal force that the pile exerts on the ground is the same for both the computer simulation and experimental results. Since the slope of this portion is dependent on the sandpile's angle of repose (eqn. (57)), it is encouraging that the computer simulation and experimental results agree. The experimental pile, however, exerted a greater horizontal shear stress near the edges of the pile than did our simulated pile.

Although we have qualitative success in modelling the form of the tangential stress, we cannot obtain the experimentally observed depression in the normal stress underneath the centre of the pile (Fig. 17(b)). Instead, eqns. (42), and (56) suggest that the normal force should be constant between  $x_c$  and  $B - x_c$ . Possible reasons for this discrepancy between our results and experiment are:

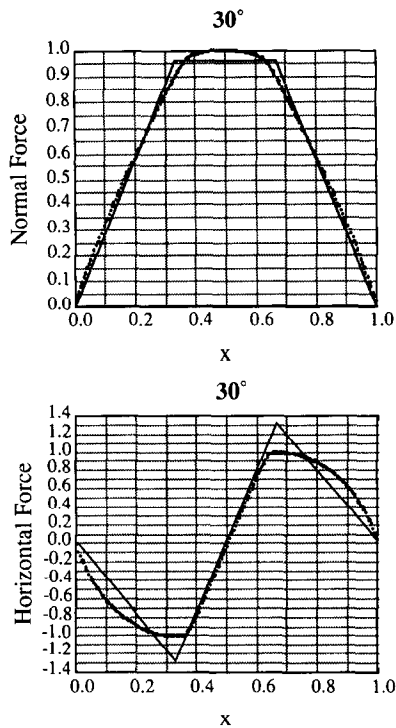


Fig. 15. We typically use piles containing 360 particles to obtain the force structure of the  $30^\circ$  piles shown in Figs. 13 and 14. To check that our results are correct, we have created a  $30^\circ$  pile consisting of 5490 particles. Comparing the relevant results, it is clear that the normalized force profiles between the small and large piles are very similar, and although the difference between the theoretical normal force and the simulation force is smaller than that obtained in Fig. 13, it is seen that the simulation results for the horizontal force between the pile and the ground do not converge to the analytic model.

(1) the experimental results are true for a three dimensional pile, while we are investigating the behaviour of a two dimensional pile,

(2) the experimental piles are not perfect cones, and

(3) real particle piles are made of nonspherical particles with different sizes, and somewhat random positions. In our theoretical analysis however, we have created our piles with a regular, close packed distribution of identical particles.

Unfortunately, our code is not yet ready to handle three dimensional structures, so this possibility will have to be investigated in our next study. We are prompted to make suggestion (2), because in Smid and Novosad [1] the authors created their sandpiles by pouring sand and fertilizer from storage containers onto a measuring platform. It is possible that the sandpiles formed via this method did not have a perfect triangular profile. For example, if the bulk solid had enough kinetic energy, it could have flattened the top of the pile (see Fig. 18(a)), or if the material had a relatively small amount of kinetic energy, it is possible that it had a peak with a slope greater than the main pile's angle of repose

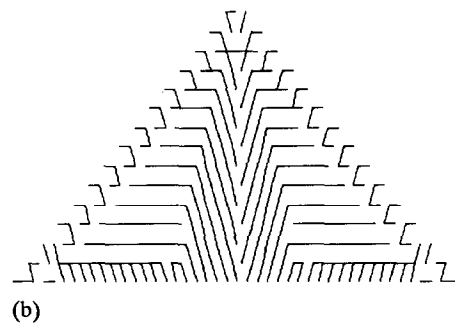
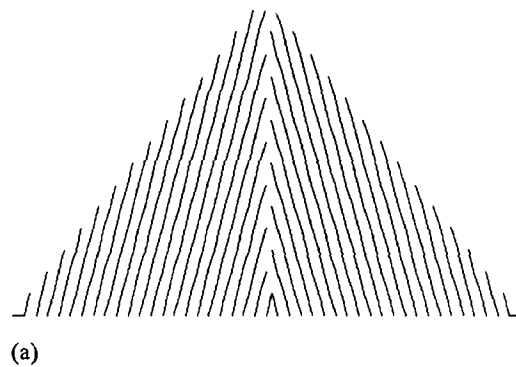


Fig. 16 (a). The lines of maximum force obtained from our discrete particle computer code for a sandpile with a  $30^\circ$  angle of repose. As in Fig. 10(a), the maximum force lines still make an angle of  $\pi/3$  or  $2\pi/3$  to the horizontal. (b). The lines of minimum force obtained from our discrete particle computer code for a sandpile with a  $30^\circ$  angle of repose. Unlike Fig. 10(b), where there were no contacts between particles on the same level, the minimum force lines now propagate horizontally between neighbouring particles, although some still make an angle of  $\pi/3$  or  $2\pi/3$  to the horizontal.

(Fig. 18(a)). To investigate this possibility, we modify our continuum triangular pile as shown in Fig. 11 to the 'tent' profiles shown in Fig. 18, but still assume that the internal forces are propagating along lines inclined at an angle of  $\pi/3$  or  $2\pi/3$  to the horizontal.

As before, we can obtain analytic expressions for the lengths  $l_1$  and  $l_2$ , but given the qualitative nature of the suggestions, it is more convenient to find the lengths numerically from the intersections of the lines  $l_1$  and  $l_2$  with the 'tent' profile. From these calculations, we found that piles with  $\alpha_1 > \alpha_2$ , (where  $\alpha_1$  and  $\alpha_2$  are the angles shown in Fig. 13) do not possess a minimum in the normal stress. However, if  $\alpha_2 > \alpha_1$  then it is relatively easy to obtain a depression in the normal force curve as shown in Fig. 19, *although this normal force curve is not replicated when we analyze the force distribution, with our simulation code, in a similarly shaped pile made of discrete particles.*

Returning to suggestion (3), we have not created sandpiles with particles of different radii, preferring, instead, to learn about simpler systems where all the particles have the same radii. But we can easily create systems where the particles have been accumulated in

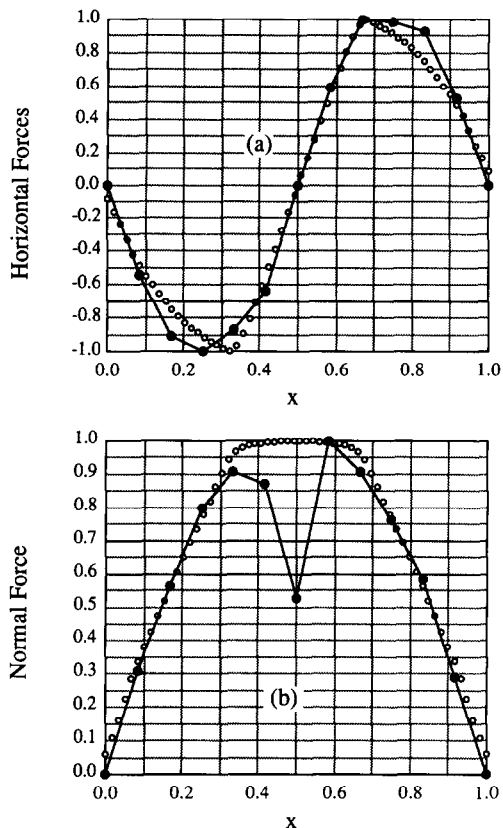


Fig. 17. Comparison of results from Smid and Novosad [1] (denoted by filled circles joined by lines) with the results from our computational model (denoted by open circles only) for a pile with a 32.6° angle of repose, which was the angle of repose for the experimental pile. Fig. 17 (a) displays the horizontal force the pile exerts on the ground, and the good agreement between the computed and experimental results. Fig. 17 (b) displays the normal force the pile exerts on the ground. The central depression in the experimental normal force is not replicated in the computer model. The possible reasons for this discrepancy are discussed in the text.

a semi-random fashion. For instance, using our discrete particle simulation code, we can create a pile of ‘soft’ particles by dropping one particle at a time. An example of just such a pile is shown in Fig. 20(a), where we also show the normal force profile in Fig. 20(b). Note that we obtain a slight depression in the centre of the normal force distribution, but not of a magnitude that is comparable to that observed by Smid and Novosad [1] (see Fig. 17). A general conclusion cannot be obtained from a sample of one; indeed, other random piles that we have created in a similar fashion show no depression in the middle of the normal force distribution.

**Conclusions**

We have attempted to replicate, by analytic and computational analysis of the force distribution in a

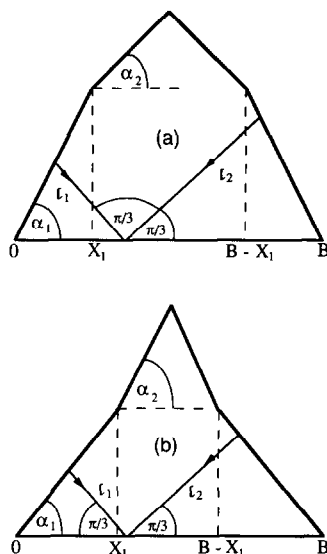


Fig. 18. ‘Tent’ profile sandpiles. In (a), we have  $\alpha_1 > \alpha_2$ , while for (b),  $\alpha_2 > \alpha_1$ . The force lines  $l_1$  and  $l_2$  make an angle of  $2\pi/3$  and  $\pi/3$ , respectively to the horizontal. The first ‘bump’ in the tent profile occurs at a distance  $X_1$  along the base of the pile, where the base length is denoted by  $B$ .

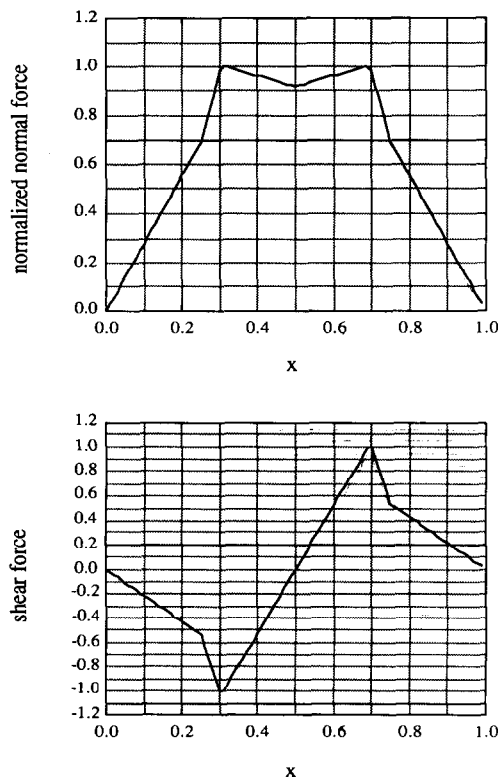


Fig. 19. The normalized horizontal and normal forces obtained from our analytic model for a ‘tent’ sandpile with a profile similar to Fig. 18 (b), where  $\alpha_1 = 30^\circ$ ,  $\alpha_2 = 45^\circ$ , and  $X_1 = 0.38B$ . Note that the dip in the normal force profile is not replicated when we analyze the force distribution for a similarly shaped pile with our discrete particle computer model.

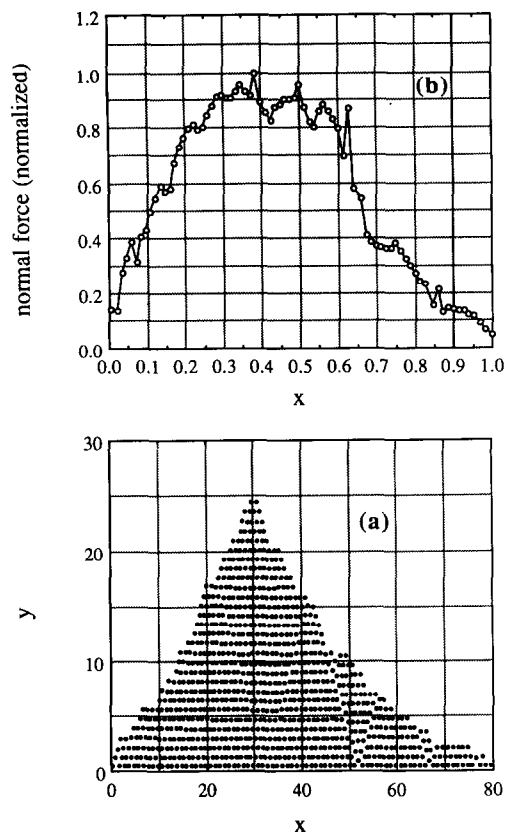


Fig. 20. In Fig. 20(a) we show a particulate pile consisting of 968 particles, which have been assembled by dropping one particle at a time from a height of two particle diameters above the highest point in the pile. As the pile grows with time, it experiences avalanches, forms 'fault' lines, and develops a more random internal structure. The normal force profile obtained at the base of the pile is shown in Fig. 20(b), although the normal force profile does dip around the middle of the pile. The relative magnitude of the depression in the normal force is small compared to what is observed experimentally.

two dimensional sandpile, the results obtained by Smid and Novosad [1] for the vertical and shear stress at the base of a conical pile of particulate material. We have successfully replicated their results for the shear

stress, but are unable to replicate the depression in the vertical stress distribution, which they showed occurred under the highest point of the pile. However, our models show that the vertical stress distribution should become constant within a certain distance of the centre of the pile.

The most probable explanation for the difference between our theoretical models and the experimental results, is, we believe, due to our use of a two dimensional model to describe a three dimensional physical system. Development of a three dimensional discrete particle code, in a future study, will hopefully shed light on this issue.

Our results suggest that in close packed particulate material, maximal force propagates along lines that make an angle of  $\pi/3$  to the horizontal. This result allows us to create a simple analytic description of forces obtained in piles of particulate material of arbitrary shape.

## References

- 1 J. Smid and J. Novosad, *I. Chem. E. Sump.*, 63 (1981) D3/V/1.
- 2 D. F. Bagster, *J. Powder Bulk Solids Technol.*, 6 (1982) 1.
- 3 D. F. Bagster and R. Kirk, *J. Powder Bulk Solids Technol.*, 9 (1985) 19.
- 4 G. R. Brooks and D. F. Bagster, *J. Powder Bulk Solids Technol.*, 8 (1984) 18.
- 5 E. Li and D. F. Bagster, *Powder Technol.*, 63 (1990) 277.
- 6 D. Greenspan, *Computer Oriented Mathematical Physics*, Pergamon Press, Oxford, 1981.
- 7 W. H. Press, B. P. Flannery, S. A. Teukolsky and W. T. Vetterling, *Numerical Recipes The Art of Scientific Programming*, Cambridge University Press, Cambridge, 1986, p. 655.
- 8 M. A. Hopkins, *Particle Simulation: Volume I, Report No. 87-7*, Department of Civil and Environmental Engineering, Clarkson university, Postdam, New York, 1987.
- 9 D. Greenspan, *J. Comput. Phys.*, 56 (1984) 28.
- 10 J. Witters and D. Duymelinck, *Am. J. Phys.*, 54 (1) (1986) 80.
- 11 P. A. Cundall and O. D. L. Strack, *Geotechnique*, 29 (1979) 47.